Room temperature bio-engineered multifunctional carbonates for CO_2 sequestration and valorization

Mohamed, H.; Hkiri, K.; Botha, N.; Cloete, K.; Azizi, Sh; Ahmed, A. A.Q.; Morad, R.; Motlamane, Th; Krief, A.; Gibaud, A.; Henini, M.; Chaker, M.; Ahmad, I.; Maaza, M.

Published in:
Scientific Reports

DOI:
10.1038/s41598-023-42905-5

Publication date:
2023

Document Version
Publisher's PDF, also known as Version of record

scientific reports

Check for updates

OPEN

Room temperature bio-engineered multifunctional carbonates for CO_2 sequestration and valorization

H. Mohamed[1,2,3], K. Hkiri[1,2], N. Botha[1,2], K. Cloete[1,2], Sh. Azizi[1,2], A. A. Q. Ahmed[1,2], R. Morad[1,2], Th. Motlamane[1,2], A. Krief[1,2,4], A. Gibaud[1,2,5], M. Henini[1,2,6], M. Chaker[1,2,7], I. Ahmad[1,2,8] & M. Maaza[1,2]✉

This contribution reports, for the first time, on an entirely green bio-engineering approach for the biosynthesis of single phase crystalline 1-D nano-scaled calcite $CaCO_3$. This was validated using H_2O as the universal solvent and natural extract of *Hyphaene thebaica* fruit as an effective chelating agent. In this room temperature green process, $CaCl_2$ and CO_2 are used as the unique source of Ca and CO_3 respectively in view of forming nano-scaled $CaCO_3$ with a significant shape anisotropy and an elevated surface to volume ratio. In terms of novelty, and relatively to the reported scientific and patented literature in relation to the fabrication of $CaCO_3$ by green nano-chemistry, the current cost effective room temperature green process can be singled out as per the following specificities: only water as universal solvent is used, No additional base or acid chemicals for pH control, No additional catalyst, No critical or supercritical CO_2 usage conditions, Only natural extract of thebaica as a green effective chelating agent through its phytochemicals and proper enzematic compounds, room Temperature processing, atmospheric pressure processing, Nanoscaled size particles, and Nanoparticles with a significant shape anisotropy (1-D like nanoparticles). Beyond and in addition to the validation of the 1-D synthesis aspect, the bio-engineered $CaCO_3$ exhibited a wide-ranging functionalities in terms of highly reflecting pigment, an effective nanofertilizer as well as a potential binder in cement industry.

Within the pressing urgency of climate change[1], de-carbonization processes and related technologies (CO_2 sequestration, CO_2 cycling, CO_2 conversion, …) are extensively investigated in view of reducing the CO_2 global footprint[2–4]. Cabonates (XCO_3) in general and Calcium Carbonate ($CaCO_3$) specifically could be effectively produced by harnessing atmospheric CO_2 and converting it into a valuable final product that is of an economical value such as a major cement component[5], white pigment[6], green fertilizer[7] or/and a drug carrier in the health sector[8,9].

$CaCO_3$ makes up almost 4% of the Earth's crust and has been studied extensively due to its importance in bio-mineralisation in natural systems, including alkalinity generation, and biogeochemical cycling of elements[7,10–12]. Indeed, natural $CaCO_3$ which forms through bio-mineralization process[13,14], has three known natural crystalline forms, vaterite, calcite, and Aragonite, the first one being a metastable poly-crystal[15–18]. However, vaterite has attracted the attention of the scientific community in view of its peculiar optical and biochemical properties[19–22], which include porosity along with practical relevance and self-assembly synthesis. Henceforth, vaterite particles are likely to be used effectively as biocompatible containers for delivering therapeutic relevant compounds into living cells and tissues[23]. Moreover, $CaCO_3$ particles can be successfully employed as templates for the synthesis of polymer hollow capsules made by using a layer-by-layer method, which are also commonly used as drug delivery carriers[24–26]. Several protocols of vaterite synthesis have been reported[19–21]. For example, the process

[1]UNESCO-UNISA Africa Chair in Nanosciences-Nanotechnology, College of Graduate Studies, University of South Africa, Muckleneuk Ridge, PO Box 392, Pretoria, South Africa. [2]Nanosciences African Network (NANOAFNET), Materials Research Department, iThemba LABS-National Research Foundation of South Africa, 1 Old Faure Road, Somerset West, PO Box 722, Cape Town 7129, Western Cape, South Africa. [3]College of Graduate Studies, University of South Africa, PRETORIA, South Africa. [4]Chemistry Department (CMI Laboratory), University of Namur, 2 Rue Joseph Grafé, 5000 Namur, Belgium. [5]IMMM, UMR 6283 CNRS, University of Le Maine, Bd O. Messiaen, 72085 Le Mans Cedex 09, France. [6]Physics and Astronomy Department, Nottingham University, Nottingham NG7 2RD7, UK. [7]INRS-Energie et Matériaux, 1650 Lionel-Boulet, Varennes, QC J3X 1S2, Canada. [8]Experimental Physics Directorate (EPD), National Center for Physics, Islamabad 44000, Pakistan. ✉email: Maaza@tlabs.ac.za; Maazam@unisa.ac.za

of crystallization of $CaCO_3$ occurring through the formation and further transformation of amorphous $CaCO_3$ into vaterite and then Calcite has been demonstrated[27]. The 2 other structures of $CaCO_3$ i.e. the Aragonite and Calcite forms of $CaCO_3$ play a pivotal role in various strategic industries, specifically cement, paint and coatings sectors[12,13,22–25,28].

From the synthesis viewpoint, and in addition to the established physical[27,29–31] and chemical[28,32,33] processes as well as the natural biomimicry for the fabrication of $CaCO_3$[34,35], there is a fast growing methodology consisting of bio-engineering such a compound in a green and sustainable approach. As such, natural systems and natural extracts of plants have been successfully used as effective chelating agents[36–46].

Within this contribution, an outright green novel bio-engineering approach for the biosynthesis of single phase crystalline nano-scaled $CaCO_3$ is validated using H_2O as the unique solvent and natural extract of *Hyphaene thebaica* fruit as an effective chelating agent. In this room temperature green process, $CaCl_2$ and CO_2 are used as the sole source of Ca and CO_3 respectively in view of forming nano-scaled $CaCO_3$ with a significant shape anisotropy and an elevated porosity.

In terms of novelty and originality, and relatively to the reported scientific and patented literature in relation to the fabrication of $CaCO_3$ by green nano-chemistry, the current cost effective room temperature green process can be singled out as per the following specificities:

i. Only water as universal solvent is used,
ii. No additional base or acid chemicals for pH control,
iii. No additional catalyst,
iv. No critical or supercritical CO_2 usage conditions,
v. Only natural extract of *Hyphaene thebaica* as an effective chelating agent via its phytochemicals and/or enzymatic compounds,
vi. Room temperature processing,
vii. Atmospheric pressure processing,
viii. No extra thermal annealing required,
ix. Nano-scaled size particles
x. Nanoparticles with a significant shape anisotropy (1-D like nanoparticles)

Experiments, results and discussions

Synthesis and methodology

Based on previous successful validation of bio-engineering of several simple and binary oxides using various natural oxides[47–58], *Hyphaene thebaica* L. Mart fruit was specifically selected in this case. This latter was considered in view of the strong chemical chelation effectiveness of its phyto-compounds. Hence and within this contribution, *Hyphaene thebaica* L. was used. The considered *Hyphaene thebaica* L. Mart fruit material was collected from Aswan, Egypt and washed in running distilled H_2O and kept in shade for drying in South Africa. The dried fruit material was grounded to fine powder and then stored at room temperature in standard zipper bags. For a typical aqueous extraction, 10 g fruit powder was added to 200 ml of dH_2O and boiled at 80 °C for 2 h on a standard laboratory hot-plate. The resultant mixture was filtered 3 times in view of obtaining a visually clear aqueous extract. The mechanism of Chelation has been discussed and presented in a series of publications[50–58].

As it will be discussed later (Section "Properties: light scattering and white pigment applications"), It is to be emphasized that the proposed green synthesis of the nano-scaled $CaCO_3$ goes through 2 major phases. The first phase consists of the chemical chelation of the $CaCl_2$ precursor by the natural extract of *Hyphaene thebaica* fruit (Likely transformation of $CaCl_2$ to $(CaOH)_2$). The second phase is related to the reaction of CO_2 bubbled gas with the chelated Ca Cl_2 i.e. $(CaOH)_2$.

Within this study, and in a typical preparation, 3.32 g of Calcium Chloride ($CaCl_2$ M = 110.98 g) were added to 100 mL filtered extract solution and stirred for 24 h at room temperature with gentle stirring and after that bubbling with CO_2. Afterwards, the precipitates from the reaction mixture were collected by allowing them to settle down. Then, the precipitate is collected by centrifugation for 20 min at 4000 rpm. The precipitate was washed thrice in dH_2O by subsequent centrifugation for 10 min at 4000 rpm, and the precipitates were washed by subsequent centrifugation for 10 min at 4000 rpm. Finally, the washed precipitate was kept for drying at room temperature. The white powder is investigated in its powdered or pelletized forms.

Materials and characterization

The scanning electron microscopy (SEM) investigations were conducted on a Verios 5 XHR SEM unit. The UV–VIS–NIR diffuse reflectance studies were acquired using an Ocean Optics unit within the spectral range of 250–1100 nm. As a standard reference for reflectance measurements, $BaSO_4$ standard was used. With an optical bandgap of ~ 6 eV, $BaSO_4$ exhibits a low absorption extending to the UV band correlated to an elevated UV–VIS and NIR reflectance. The Luminescence measurements were recorded using a fibre-optics linked Ocean Optics system consisting of a UV light-emitting diode source coupled to a high sensitivity QE Pro-FL spectrophotometer. The excitation wavelength was fixed at 240 nm. The X-rays Diffraction measurements were carried out with a Bruker D8 equipped with a copper sealed tube x-ray source producing Cu - $K_{\langle 1}$ radiation at the wavelength of 1.5406 Å from a generator operating at 40 keV and 40 mA (operating at Θ–2Θ configuration). The scanning rate was 0.03° 2Θ per minute from 20° to 85°. The Diffraction patterns were interpreted using MAUD software.

The Thermal Gravimetry Analysis (TGA) and Differential Scanning Calorimetry (DSC) experiments were performed using a Mettler Toledo TGA/DSC 1 Stare System analyser with a horizontal reaction chamber. About 10–20 mg of sample were placed in a cylindrical Al_2O_3 crucible. The TGA furnace was constantly purged with Ar gas. The samples were annealed from 25 to 900 °C at a heating rate of 10 °C/min in a stream of N_2 or Ar "reactive

gas" provided directly above the sample with a flow rate of 50 mL min^{-1}. A baseline, obtained under the same conditions with an empty Al_2O_3 crucible, was subtracted from the measured thermograms. The Luminescence measurements were recorded using a fibre-optics linked Ocean Optics system consisting of a UV light-emitting diode source coupled to a high sensitivity QE Pro-FL spectrophotometer. The excitation wavelength was fixed at 240 nm.

Morphological investigations

Figure 1 reports a typical high resolution transmission electron microscopy (HRTEM) and Selected Area Electron Diffraction (SAED) of the bio-engineered $CaCO_3$. The particles exhibit nano-scale size and a crystal-clear shape anisotropy in a form of 1-D tubular nanorods with sharp truncated end facets in general (Fig. 1a). Their basal diameter as well as their longitudinal dimension are relatively polydisperse. A typical Basal and longitudinal dimensions of such nanorods are $ø_{Basal} \sim 94$ nm and $D_{Long} \sim 1473$ nm. But they can be longer (> 1µm) (Fig. 1d). However, a low magnification observations (Fig. S1a) seem indicating that the $CaCO_3$ rods' basal diameter is relatively disperse size wise. In some cases, they form bundles. Figure S1b reports the normalized basal size distribution. It indicates that the basal dimension of the $CaCO_3$ rods varies within the range of 50–800 nm with a relatively large population within the 50–300 nm range.

One should point out that such nanorods seem to be porous. Some nanorods seem, even, exhibiting a hollow longitudinal pores along along their axis (Fig. 1b,c). To sustain the existence of such a porosity, BET investigations were carried out. Figure S2a reports the corresponding profiles. More precisely, Fig. S2b displays the N_2 adsorption/desorption curves exhibiting the standard isotherm behaviour with a hysteresis-like evolution starting within the vicinity of $p/p_0 \sim 68\%$. Figure S2a reports a relatively narrow pore distribution of the $CaCO_3$ nanorods peaking at about 8.63 nm.

From crystallographic perspective, and as shown in Fig. 1c,d, the biosynthesized $CaCO_3$ are not amorphous but crystalline. While the majority of the 1-D tubular $CaCO_3$ are polycrystalline (Fig. 1e), some are significantly textured exhibiting an intense spot like electron diffraction pattern (Fig. 1f) as observed previously by Andrews et al.[59] and Markgraf et al.[60].

Elemental analysis and chemical composition

Figure 2 displays a typical Scanning Electron Spectroscopy (EDS) profile of the bio-engineered nano-scale $CaCO_3$. It reveals 5 major peaks centred at various energy channels of ~ 0.04, ~ 0.27, ~ 0.52, ~ 3.96 and ~ 4.02 keV. According to the EDS database, they are attributed to C, Ca, O, Ca, Ca and Ca respectively (The C peak is attributed to the Carbon coating required for for the EDS investigation). In addition to these intense peaks, and yet they are at the background level, one could observe 2 additional peaks located at ~ 1.78 and ~ 1.94 keV which might

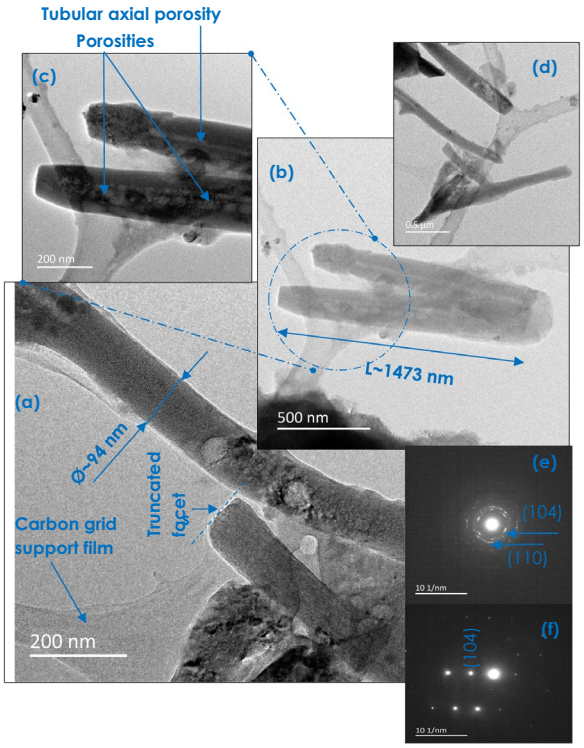

Figure 1. Typical high resolution transmission electron microscopy (HRTEM) and selected area electron diffraction (SAED) of the bio-engineered $CaCO_3$.

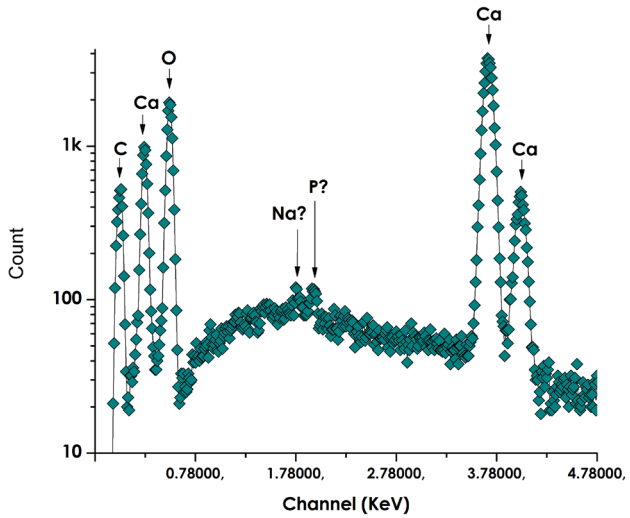

Figure 2. Typical scanning electron spectroscopy (EDS) profile of the bio-engineered nano-scaled $CaCO_3$.

be assigned to Na, K and/or P. These later contaminant elements originate likely from the natural extract itself as it was observed in various other oxides bio-synthesized via natural extracts as in the case of bulk $CaCO_3$[47–49]. These elements are characterized by a relatively small ionic radius and fast diffusion within any potential channels within the synthesized $CaCO_3$.

Thermogravimetry analysis

Figure 3a reports the Thermo Gravimetry Analysis (TGA) of the bio-engineered nano-scale $CaCO_3$ within the thermal range of 25–900 °C. There are, a priori, 2 major decompositions taking place at about ~ 109.3 and ~ 648.8 °C respectively. The first one is likely to be related to H_2O molecules adsorbed onto the surface, outer or inner interfaces and/or the porosities of the nano-scaled $CaCO_3$.The second one, taking place at the vicinity of ~ 648.8

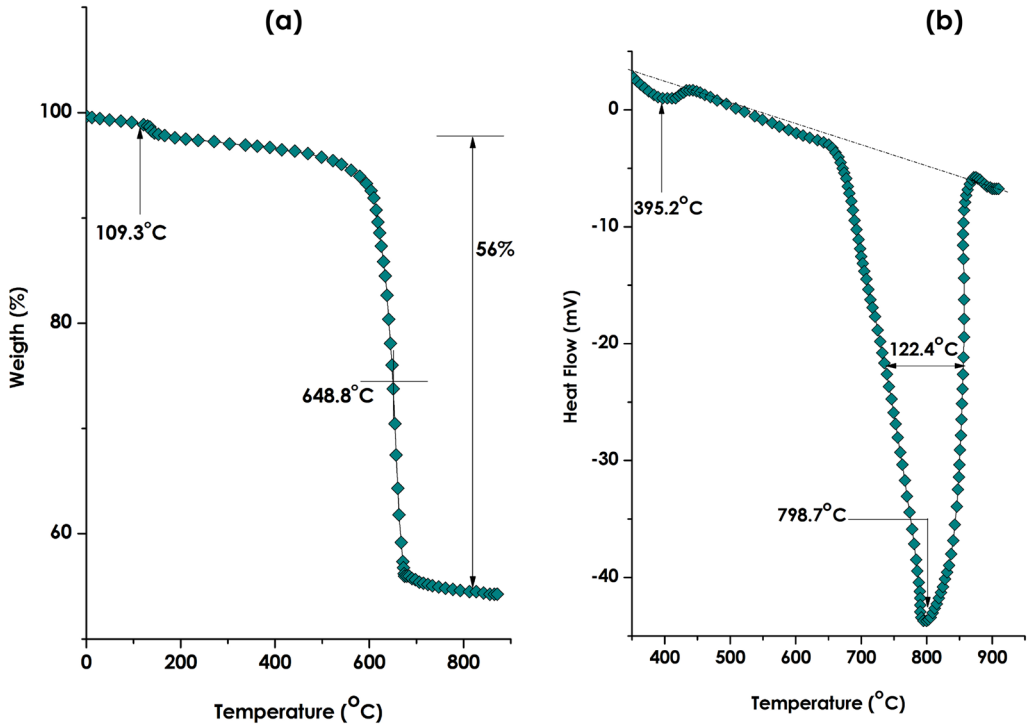

Figure 3. (**a**) Thermo gravimetry analysis (TGA) of the bio-engineered nano-scale $CaCO_3$ within the thermal range of 25–850 °C, (**b**) the corresponding differential scanning calorimetry (DSC) profile within the thermal range of 25–900 °C.

°C, is likely related to the decomposition mechanism of $CaCO_3$ corresponding to 56% in weight loss. Following such, CaO crystals and gaseous CO_2 are formed according to $CaCO_3(s) \rightarrow CaO(s) + CO_2(g)$[61].

Figure 3b reports the Differential Scanning Calorimetry (DSC) profile within the thermal range of 25–900 °C. One can distinguish 2 major exothermic phase transitions centred approximately at ~ 395.2 and ~ 798.7 °C. Both phase transitions are not 1st order type considering their width at half maximum which are about $\Delta T_{1/2}$ (395.2 °C) ~ 103.7 °C and $\Delta T_{1/2}$ (798.7 °C) ~ 122.4 °C. One should point to the absence of the exothermic peak of $Ca(OH)_2$ normally taking place around ~ 400 °C. This indicates that the formation of $CaCO_3$ is complete without, a priori any trace of the intermediary compound $Ca(OH)_2$[61].

Compared to literature, while the general TGA and DSC evolutions/trends are, grosso-modo, equivalent to that of bulk $CaCO_3$ but with a significant shift to lower temperatures. More accurately, the decomposition and phase transition temperature are ~ 648.8 °C instead of ~ 750 °C for Bulk[61]. This is likely due to the high surface to volume ratio of the current nanoscaled $CaCO_3$ comparatively to their bulk equivalent.

Vibrational properties: Raman and Fourier transform infrared spectroscopy investigations

Figure 4a displays the room temperature Fourier Transform Infrared spectroscopy spectrum of the bio-engineered nano-scale $CaCO_3$ within the spectral range of 400–4500 cm^{-1}. One can distinguish several absorption bands. These later are centered approximately at 3713.5, 2857.8, 2519.7, 1792.5, 1314.5, 866.6, 713.5 cm^{-1}. Excluding those centered at 866.6 and 713.5 cm^{-1}, the rest which are relatively broad absorptions, are related to O–H modes, C–H streching, O–H modes, C=O stretching and C–H bending vibrational modes. The singular sharp ones positioned at about 866.6 cm^{-1} and 713.5 cm^{-1} are proper to $CaCO_3$. More precisely, while the one localized at 866.6 cm^{-1} is a characteristic of the O-CO_3^2 vibrational mode in calcite. It is to be highlighted that samples containing CO_3^{2-} groups, as the case of $CaCO_3$, usually exhibit a doublet associated to the v3 vibrational mode close to 1400–1500 cm^{-1} in FTIR. The band with two shoulders clearly visible close to this region are in fact the doublet of CO_3^{2-}[62–64]. The singular absorption at 713.5 cm^{-1} is proper to the Ca–O vibrational mode in calcite and not in aragonite nor vaterite phases as highlighted in the zoom of Fig. 4b[65]. Indeed, and as per the precise investigations of Vagenas et al.[65], the Ca–O mode's infrared absorption bands are positioned at 713 cm^{-1} for calcite, 745 cm^{-1} for vaterite, and 700 cm^{-1} for aragonite[65].

Figure 5a reports the room temperature Raman spectrum of the bio-engineered $CaCO_3$ nanoparticles within the range of 0–1200 cm^{-1}.One can distinguish 4 major peaks centered approximately at the vicinity of ~ 161, ~ 288, ~ 718 and ~ 1091 cm^{-1}. While the 161 mode is a Transversal vibrational mode common to both Calcite and Aragonite, the mode located at 288 cm^{-1} is a longitudinal vibration mode characteristic of calcite. More precisely, while the mode at ~ 1091 is an A_{1g}, those centered at 161, 288 and 718 cm^{-1} correspond to E_g modes of the calcite phase[53]. One should mention however that the rhombohedral primitive cell of calcite contains 2 $CaCO_3$ formula units, for a total of 10 atoms; its 27 vibrational modes can be classified according to the irreducible representations of the 3 m point group as follows: $\Gamma_{total} = 1A1g \oplus 2A1u \oplus 3A2g \oplus 3A2u \oplus 4Eg \oplus 5Eu$.

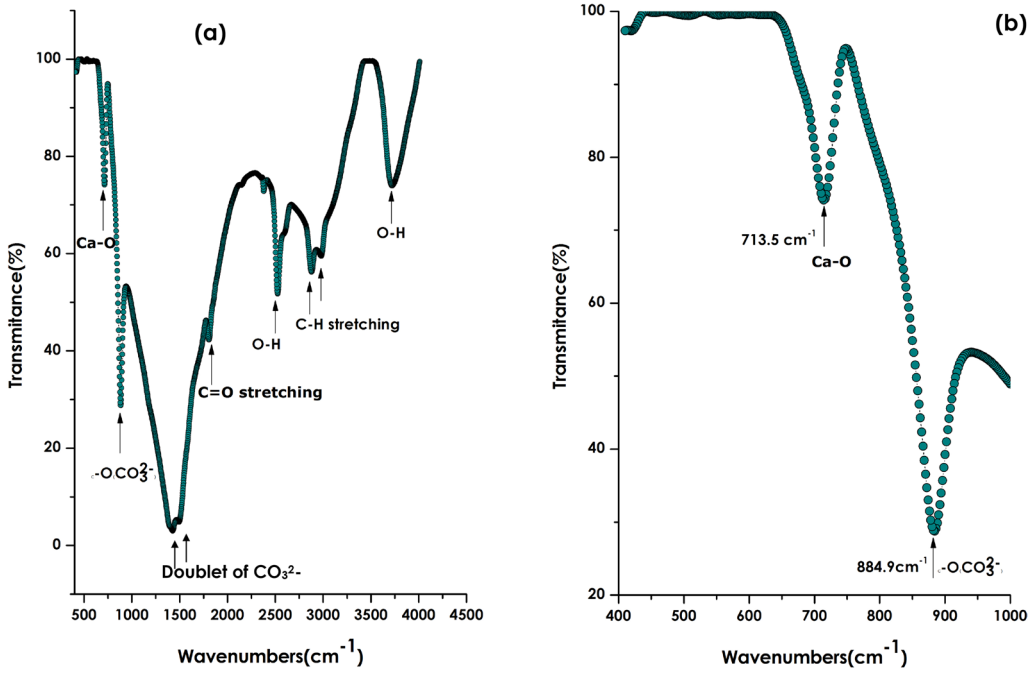

Figure 4. (**a**) Room temperature Fourier Transform Infrared spectroscopy spectrum of the bio-engineered nano-scale $CaCO_3$ within the spectral range of 400–4500 cm^{-1}, (**b**) zoom on the spectral region of 400–1000 cm^{-1} reporting the characteristic Raman active modes of Calcite $CaCO_3$ at 288 cm^{-1} ($L_{Calcite}$) and 161 cm^{-1} ($T_{Calcite}$).

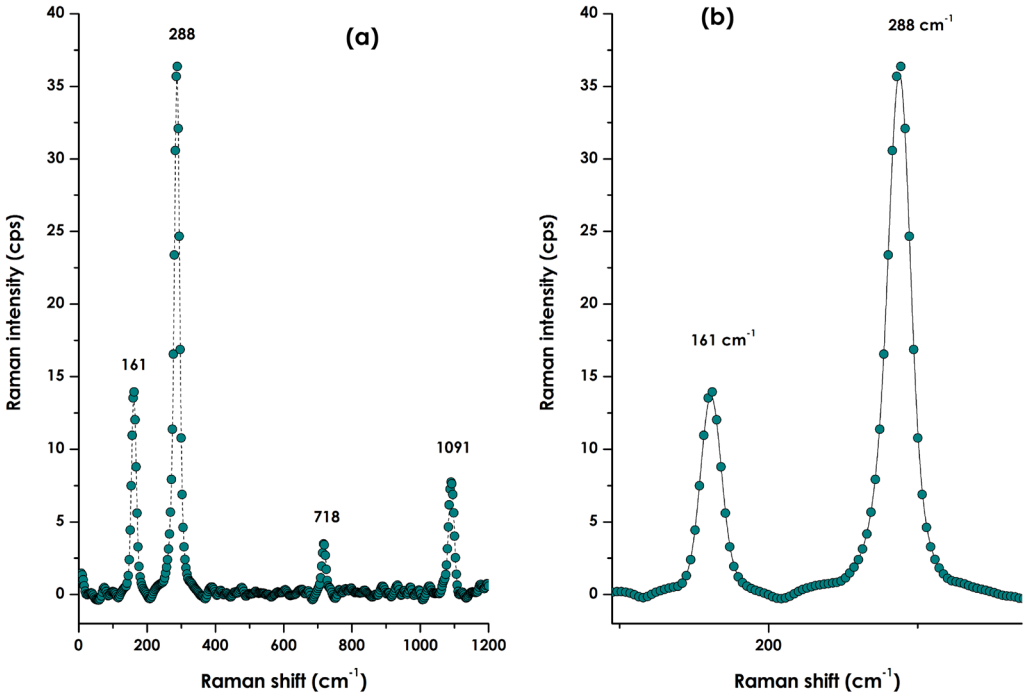

Figure 5. (**a**) Room temperature Raman spectrum of the bio-engineered $CaCO_3$ nanoparticles within the range of 0–1200 cm^{-1}, (**b**) zoom on the spectral region of 100–370 cm^{-1} reporting the Ca-O characteristic vibrational mode of Calcite $CaCO_3$.

A_{1g} and E_g (double degenerate) modes are Raman active, A_{2u} and Eu (double degenerate) are IR active, A_{1u} and A_{2g} are spectroscopically inactive (silent modes).

Last not least, and as highlighted in the zoom of Fig. 5b, one should notice the clear-cut absence of any additional Raman peak between 288 cm^{-1} ($L_{Calcite}$) and 161 cm^{-1} ($T_{Calcite}$) especially the distinctive $L_{Aragonite}$[66]. Consequentially, one could safely conclude that the bio-engineered $CaCO_3$ nanoparticles are of pure single phase calcite nature.

Defects investigations: photoluminescence studies

Figure S3a reports the spectral emission of the exciting source, the excitation source consists of major emissions centered at 242.7, 263.5, 281.5, and 318.5 nm. Figure S3b displays the mission of the *Hyphaene thebaica* powder used as an effective chelating agent. It consists of a relatively minute emissions centered at 508.2 and 581.5 nm. Figure 6 displays the room temperature photoluminescence of the bio-synthesized nanoscaled $CaCO_3$ (well as the intermediary product of $Ca(OH)_2$ as well as the initial precursor $CaCl_2$ under the external excitation of Fig. S3a. Each and all exhibit a major broad emission centred at about ~ 490.1 nm, ~ 496.9 and ~ 507.2 nm for $CaCl_2$, $CaCO_3$ and $Ca(OH)_2$ respectively. In view of the spectral position similarly of the maximum emission, this later is likely to be of the same physical origin. Such a broad emission of the Bio-engineered $CaCO_3$ could be caused by surface or volume Ca defects or recombination of electrons of (Ca^+-CO_3.)-centres for the intrinsic emission band[67,68]. Likewise, it can be caused by the intrinsic emission of the electron–hole recombination where a CO^{3-} ion plays the role of the hole and Ca^+ the role of the electron[69–72].

Crystallographic studies

As established, in standard P–T conditions, $CaCO_3$ has three polymorphs: calcite (rhombohedral), Aragonite (orthorhombic), and Vaterite (orthorhombic). Calcite is thermodynamically the most stable in most environments[61,65]. Figure 7a,b display the Θ–2Θ X-rays diffraction spectra within the angular range of 20°–50° and 55°–85° respectively. 16 observed Bragg peaks were observed as summarized in Table 1. The most intense is the one centred at 29.45° which is the most intense characteristic (104) reflection of the Calcite so is the case of each and al Bragg diffraction peaks. Following the MAUD treatment. The simulation of the full spectrum (Fig. 7c), the derived lattice parameters are ⟨a⟩ = ⟨b⟩ = 4.883 Å and ⟨c⟩ = 16.310 Å. Within the experimental bar errors, these parameters are in agreement with pure Calcite trigonal crystallographic structure (Fig. 7d) with a space group R-3c[61,73]. One should mention that the lattice parameters of the 3 major phases in their bulk configuration are as follows:

Bulk Calcite trigonal: ⟨a⟩ = ⟨b⟩ = 4.9892 Å and ⟨c⟩ = 17.06089 Å, Space group R-3c.

Bulk Aragonite orthorhombic: ⟨a⟩ = ⟨b⟩ = 4.9803 Å and ⟨c⟩ = 17.0187 Å.

Bulk Vaterite orthorhombic: ⟨a⟩ = ⟨b⟩ = 4.1226 Å and ⟨c⟩ = 8.4653 Å, Space group $P6_3/mmc$.

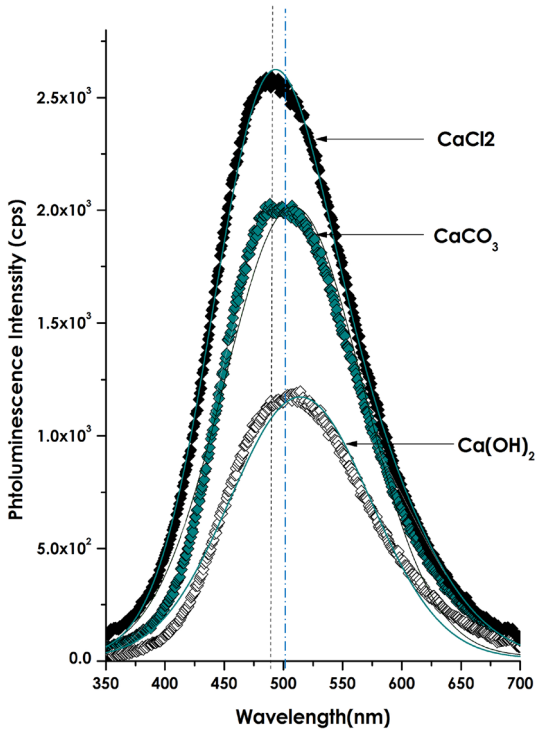

Figure 6. Room temperature photoluminescence of the bio-synthesized nanoscaled $CaCO_3$ as well as the intermediary product of Ca(OH)2 as well as the initial precursor $CaCl_2$.

In addition, the derived lattice parameters ($\langle a\rangle = \langle b\rangle = 4.883$ Å, $\langle c\rangle = 16.310$ Å) are smaller than their corresponding bulk values, suggesting that the CaCO3 nanorods are under a compressive stress within the 3 crystallographic directions.

Ethical approval

In view of the usage of the usage of "*Hyphaene thebaica* L. mart fruit" for scientific purpose, a full permission to collect it was allowed and its usage was permitted. Likewise, It is to point to the fact that the usage of the collected "*Hyphaene thebaica* L. mart fruit" complies with UNISA and iThemba LABS-National Research Foundation of South Africa institutional, national, and international guidelines and legislation.

R&D translations: potential technological applications

Properties: light scattering and white pigment applications

Figure S4 displays the UV–VIS–NIR optical absorbance of the *Hyphaene thebaica* natural extract, the extract with the $CaCl_2$ (just upon dissolution), the extract with the $CaCl_2$ (after reaction over 24 h and formation of colloidal $Ca(OH)_2$), extract with the $CaCl_2$ (after reaction over 24 h and formation of colloidal $Ca(OH)_2$ and bubbling with CO_2). Following the CO_2 bubbling, the $Ca(OH)_2$ colloidal solution becomes turbid which was interpreted as related to the formation of colloidal $CaCO_3$. As one can notice in Fig. S4a and its zoom (Fig. S4b, while the various solutions exhibit a broad optical absorbances from 200 to 400 nm, the colloidal $CaCO_3$ solution exhibit a relatively sharper absorbance in the deep blue region (200–230 nm) in addition to a constant plateau over 230 nm. The observed behavior is characteristic of pure $CaCO_3$'s absorbance[74]. Likewise, such a specific absorbance peak within the 200–230 is in line with the CaCO3's bandgap of about 5 eV.

To sustain such an hypothesis, the 2 last colloidal solutions (after reaction over 24 h and formation of Ca(OH)2), and (after reaction over 24 h, formation of Ca(OH)2 and bubbling with CO_2) were centrifuged. Figure S5 display the corresponding UV–VIS–NIR diffuse reflectances. Both spectra are in line with the pure $Ca(OH)_2$ and $CaCO_3$[75].

Figure 8a displays the standard diffuse reflectance spectrum under normal incidence of the bio-engineered $CaCO_3$ nanoparticles (in their pelletised powder form) within the spectral range of 200–1000 nm. Figure 8b displays the corresponding zoom on the UV-Bleu spectral region of 200–345 nm. From Fig. 8a, one can safely state that there are 2 major regions, separated approximately at 300.1 nm, above which the average diffuse reflectivity is about ~ 83.7%. Such an elevated reflectivity within the visible (VIS) and Near infrared (NIR) solar spectral regions is a characteristic of highly reflecting solar materials equivalent to that of standard white pigments including $BaSO_4$, ZnO and TiO_2[76]. Henceforth, one could safely conclude that the bio-engineered $CaCO_3$ nanoparticles could be a potential compound for white pigment coatings' applications.

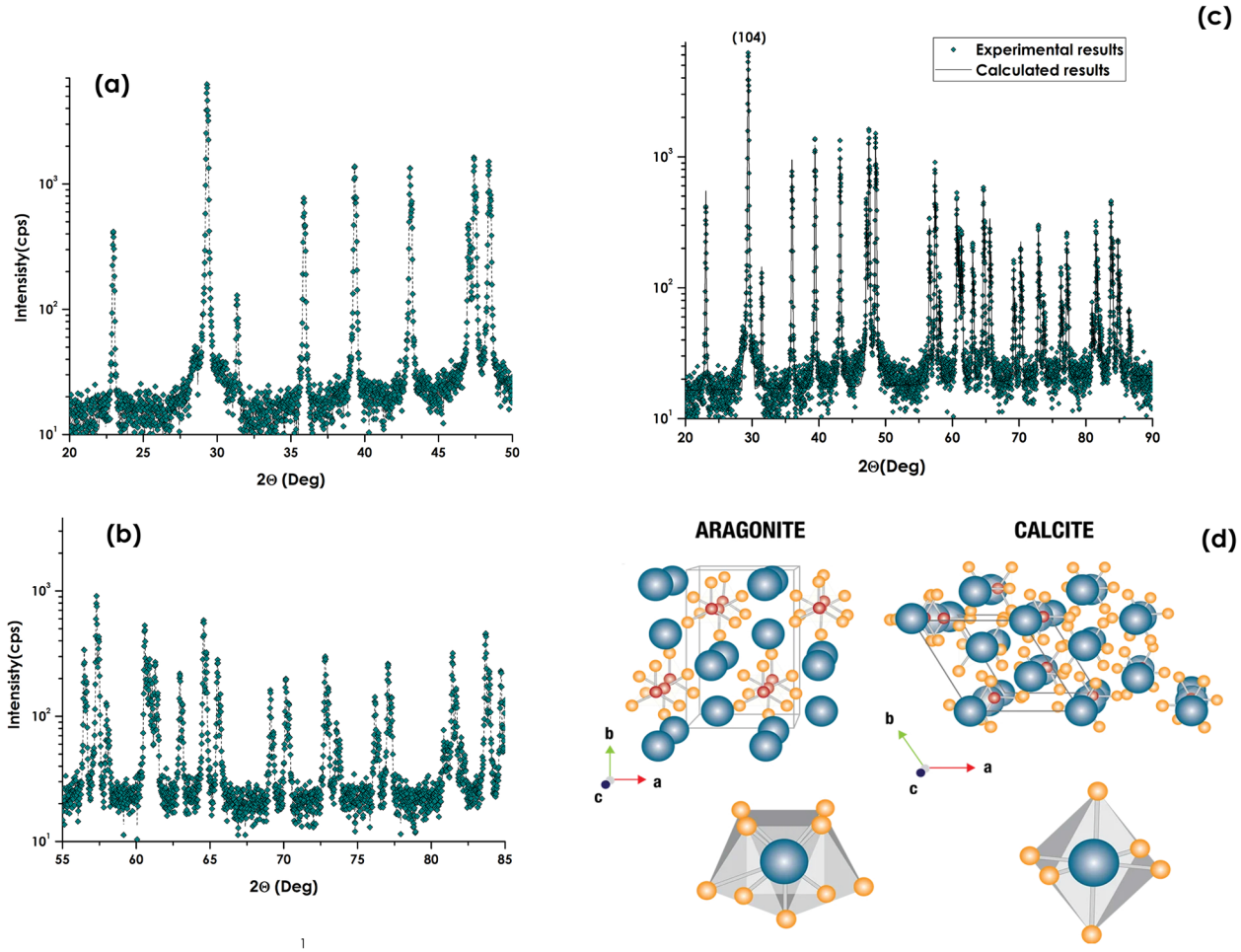

Figure 7. The Θ–2Θ X-rays diffraction spectra within the angular range of (**a**) 20°–50° and (**b**) 55°–85°, (**c**) full XRD profile with the MAUD simulation and (**d**) proposed calcite crystallographic structure of the bio-engineered $CaCO_3$ 1-D nanoparticles.

Angular position of the main Bragg peaks 2Θ (°)	Miller indexation (hki)	Corresponding $CaCO_3$ phase
22.95	012	Calcite only
29.45	104	Calcite + aragonite
31.46	006	Calcite only
36.06	110	Calcite only
39.51	113	Calcite only
43.14	202	Calcite only
47.54	018	Calcite only
48.70	116	Calcite only
56.62	211	Calcite only
57.51	112	Calcite only
60.76	214	Calcite only
64.80	300	Calcite only
73.01	128	Calcite only
77.43	220	Calcite only
81.67	214	Calcite only
83.95	134	Calcite only

Table 1. Angular position of the various Bragg diffraction peaks and their corresponding miller indexation of the bio-engineered $CaCO_3$ nanorods.

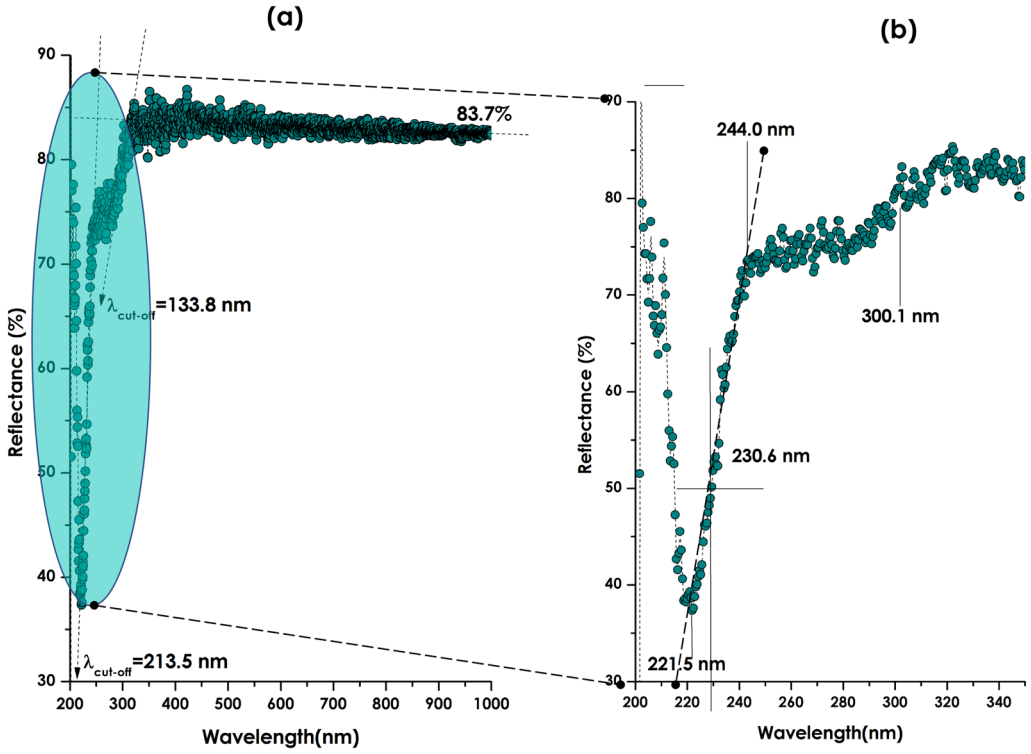

Figure 8. (**a**) Standard diffuse reflectance spectrum under normal incidence of the bio-engineered $CaCO_3$ 1-D nanoparticles within the spectral range of 200–1000 nm, (**b**) the corresponding zoom on the UV-Bleu spectral region of 200–345 nm.

If one considers the zoom of Fig. 8b, one could single out the minimum in the diffuse reflectance centred approximately at about ~ 221.5 nm with a reflectivity as low as 37.5% and the region delimited between 244.0 nm and 301.1 nm. If one consider the cut-off wavelengths $\lambda_{cut\text{-}off}$ as defined as the limit between the low and high reflectivity regions, then the value of $\lambda_{cut\text{-}off}$ could be approximated as defined by the intersection of the slope with the wavelength x-axis as indicated in Fig. 8a (dashed line intersecting the x-axis). Such an intersection is ~ 213.5 nm. If so, one could associate an optical bandgap of $E_g = hc/(\lambda_{cut\text{-}off} = 6.42$ eV ($\lambda_{cut\text{-}off} \sim 213.5$ nm) (h, Plank's constant and c, Celerity of light). This latter value of $E_g = 6.42$ eV is not far from the experimental bulk Calcite value of 6.0 ± 0.35 eV[77,78].

Properties: nanofertilizing response

As in the case of Zinc, Calcium is a crucial plant nutrient playing a vital role in maintaining plant cellular metabolism. As a biocatalyst becoming functional through Calcium ionic species, These Calcium ionic species are concerned with hydrocarbons metabolism, maintenance of cellular membranes, leaf morphology, physiology of membrane, protein production,…[79]. Likewise, it is established that Ca^{2+} activates various types of enzymes, hence is a pivotal co-factor within the plant system. More precisely, It participates in membrane transport metabolisms, nitrate take-up and in biomass proportion[79] and photosynthetic rate[80–82]. In addition, it has been demonstrated that Ca^{2+} enhances the saltiness and improves the plant development[83–85]. Calcium is found in upwards of 80 compounds some of the time called calcium salts, primarily, calcium carbonate. $CaCO_3$ is an essential part of the nursery lime, otherwise called agrarian lime. In addition, holding limit of acidic soils. $CaCO_3$ sources, for example, limestone and chalk, alongside other synthetic compounds are utilized in the readiness of agrarian lime.

In view of investigating the effectiveness of the currently bio-engineered $CaCO_3$ nanoparticles, they were tested as a bio/nano-fertilizer in the case of *Lycopersicum esculentum* (Tomato). In this regard, a similar study with the same parameters and growth conditions was performed as the one conducted previously with ZnO nanoparticles[68]. For the current study, 3 solutions of the nano-scaled $CaCO_3$ colloidal solutions were prepared at various concentrations (0.01, 0.03 and 0.05 g/l) with a reference plant as the control, 3 other *Lycopersicum esculentum* plants were considered. These latter were fed regularly with the colloidal solutions while the control one was fed with pure water only.

Accordingly, the average plant's height, the average number of leaves as well as the average number of days to flowering were collected. Table 2 summarizes such a set of results.

Figure 9a displays the evolution of the average of plant's height versus the $CaCO_3$ nutrient concentration. As one can, crystal clearly observe that the plant's height is higher than that of the control one for each of the $CaCO_3$ nutrient's concentration especially for the lowest value of 0.01 g/l. A similar behaviour is observed for the average number of leaves vs nutrient concentration (Fig. 9b). Figure 9c seems to be of a special interest. It indicates that

$CaCO_3$ concentration (g/l)	Average plant's height (± 5 mm)	Average number of leaves (± 20)	Average number of days to flowering
Control	23.1	68	118
0.01	32.7	157	94
0.03	34.1	103	104
0.05	27.2	79	108

Table 2. Evolution of the Lycopersicum *esculentum* plants' versus the $CaCO_3$ nutrient concentration and the control sample.

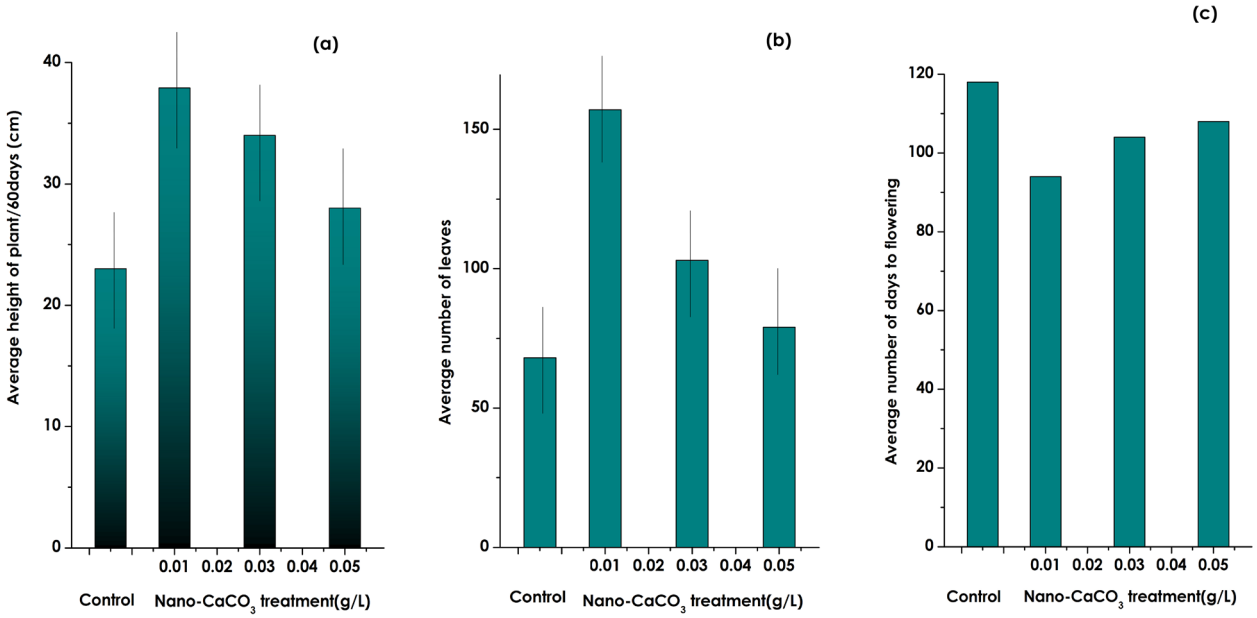

Figure 9. Evolution versus the bio-engineered $CaCO_3$ 1-D nanoparticles. Nutrient concentration of (**a**) the average of plant's height, (**b**) the average number of leaves and (**c**) the average days to flowering relatively to the control sample.

the average days to flowering is lower with the $CaCO_3$ nutrient concentration relatively to the control sample. Especially for the 0.01 g/l, the flowering is 24 days before the control. As a pre-conclusion, the plant's growth parameters are far competitive relatively to the control especially for the lowest concentration of 0.01 g/l which seems the optimal value within this conditions of experimentation.

Properties: cement binder applications

Within the building sector, especially via cement within which $CaCO_3$ is a pivotal chemical component, it is established that $CaCO_3$ contributes increasing the concrete's strength and its workability[86–89]. It also improves the concrete's particle packing while providing concrete with a spacer effect, and promotes self-compacting properties of concrete[90–92]. In addition, $CaCO_3$ reduces porosity and air void in concrete and adds to smoother surfaces[87]. From cost effectiveness viewpoint, $CaCO_3$ can be used as a filler in Portland cement, reducing the product's high cost. It was evidenced that replacement of cement by just 2% $CaCO_3$ helps reduce the CO_2 emission from cement plants by 69%, meeting the economic and environmental aspects of fly ash as well as contributing equal positive effects to concrete[93–95].

As per Fig. 1, the bio-engineered $CaCO_3$ is nano-scaled in size, and hence has a finer particles size as compared to the Ordinary Portland Cement (OPC) particles (which is in the range of 10µm in average)[95]. This fine aspect would likely improve the particle packing of concrete and give a superior spacer effect. Also, the concrete with $CaCO_3$ replacement possess a higher slump, which increases the workability. In addition, in a statistical spatial distribution, the 1-D morphology of the $CaCO_3$ nanoparticles would favour if not enhance the local mechanical strength of the $CaCO_3$/Cement composite as a local reinforcer. Last but not least, the porosity of the $CaCO_3$ nanorods (Fig. 10) could, a priori, favour an enhanced binding in view of the high surface to volume of the individual porous $CaCO_3$ nanorods.

Also, as it was mentioned previously (Sect. "Thermogravimetry analysis"), compared to literature, the general TGA and DSC variations/trends of the bio-engineered $CaCO_3$ are, equivalent to that of bulk $CaCO_3$ but with a significant shift to lower temperatures. More accurately, the decomposition and phase transition temperature are ~ 648.8 °C instead of ~ 750 °C for Bulk. This is likely due to the high surface to volume ratio of the current

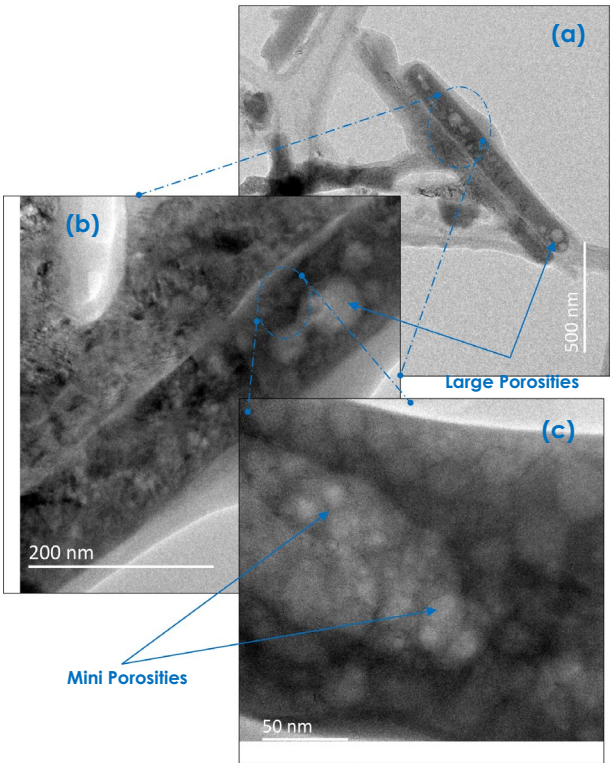

Figure 10. Multi-scale porosity in the bio-engineered $CaCO_3$ 1-D nanoparticles.

nanoscaled $CaCO_3$ comparatively to their bulk equivalent[96,97]. This would improve its workability within the cement composite.

In view of sustaining the above mentioned cement applications, a mixture of the $CaCO_3$ nano-rods with standard Ordinary Portland Cement (OPC) particles will be performed. Their mechanical and thermogravimetric properties will be investigated accordingly including early degradation in harsh environments.

One should highlight that Aragonite needle-like particles were synthesized by bubbling CO_2-containing gas into $Ca(OH)_2$ aqueous slurry in the presence of a significant amount of $MgCl_2$[98]. It was elucidated that calcite needle-like particles can be fabricated by calcining aragonite needle-like particles at 500 °C. This fabrication method of thermodynamically stable calcite needle-like particles may broaden the applications of calcium carbonate as a filling material.

It is to been emphasized that similar green approaches have been validated previously by Wang et al.[99], Nakayama et al.[100], Babou-Kammoe et al.[101] as well as Watanabe et al.[102]. More precisely, Wang et al. have used Fucoidan-mediated compound with Sodium carbonate in addition to CaCl2 mixed with a fucoidan solutions. In the case of Nakayama et al., amorphous calcium carbonate, $CaCl_2$ aqueous solution with PAA and Na_2CO_3 aqueous solution. In the case of Babou-Kammoe et al., several starting materials were used including Sodium carbonate (Na_2CO_3), sodium hydroxide (NaOH) and calcium nitrate tetrahydrate ($Ca(NO_3)_2$, $4H_2O$). Watanabe et al. have used also several precursors such as Calcium chloride powder and ammonium aqueous solution. While, the above methodologies have their merit as potentials ways, the require a relatively larger set of precursors while the proposed one requires H_2O as the universal solvent and $CaCl_2$ as the sole precursor. A priori, this later can be any Ca salt. Likewise, and as it would be reported soon, this presented room temperature green approach.

Conclusions

This study validated the possibility of green bio-engineering of 1-D single phase calcite $CaCO_3$ porous nano-rods. The bio-synthesis is performed at room temperature with H_2O as universal solvent with $CaCl_2$ and CO_2 as the unique source of Ca and CO_3. The bio-engineered nano-scaled $CaCO_3$ exhibited an effective multi-functionality including a significant efficiency as white pigment, an effective response as a nano-fertilizer and a potential source for green cement and cement industry. The same approach is likely valid for the synthesis of various Carbonates including but not limited to, $FeCO_3$, $CuCO_3$, $MgCO_3$, $NiCuO_3$, $SrCuO_3$,… Yet the natural extract of *Hyphaene thebaica* L. Mart fruit was used as an effective chelating agent at room temperature, it is safe to confirm that natural extract of other plants with equivalent phyto/enzymes composition would also be effective for the bio-synthesis of Carbonates.

Data availability

The datasets used and/or analysed during the current study available from the corresponding author on reasonable request.

Received: 21 March 2023; Accepted: 15 September 2023
Published online: 05 October 2023

References

1. Toavs, T. R. *et al.* A 30-year dataset of CO_2 in flowing freshwaters in the United States. *Sci. Data* **10**(20), 2023. https://doi.org/10.1038/s41597-022-01915-0 (2023).
2. Franta, B. Early oil industry knowledge of CO_2 and global warming. *Nat. Clim. Chang.* **8**, 1024–1025 (2018).
3. Beck, L. Carbon capture and storage in the USA: The role of US innovation leadership in climate-technology commercialization. *Clean Energy* **4**(1), 2–11. https://doi.org/10.1093/ce/zkz031(2020) (2020).
4. Salzmann, M. Global warming without global mean precipitation increase?. *Sci. Adv.* **2**, 6. https://doi.org/10.1126/sciadv.1501572 (2016).
5. McDonald, L., Glasser, F. P. & Imbabi, M. S. A new, carbon-negative precipitated calcium carbonate admixture (PCC-A) for low carbon portland cements. *Materials (Basel).* **12**(4), 554 (2019).
6. Kalafati K., & Christidis G. E., Replacement of TiO_2 pigment by $CaCO_3$, *Bulletin of the Geological Society of Greece* Vol. XXXX. In *2007 Proceedings of the 11th International Congress,* (2007)
7. Stocks-Fischer, S., Galinat, J. K. & Bang, S. S. Microbiological precipitation of $CaCO_3$. *Soil Biol. Biochem.* **31**, 1563–1571 (1999).
8. Chu, D. H. *et al.* CO_2 mineralization into different polymorphs of $CaCO_3$ using an aqueous-CO_2 system. *RSC Adv.* **3**, 21722–21729 (2013).
9. Cai, A. *et al.* Direct synthesis of hollow vaterite nanospheres from amorphous calcium carbonate nanoparticles via phase transformation. *J. Phys. Chem. C* **112**, 11324–11330 (2008).
10. Kim, Y. Y. *et al.* A critical analysis of calcium carbonate mesocrystals. *Nat. Commun.* **5**, 1 (2014).
11. Mitchell, A. C. & Te Ferris, F. G. Infuence of *Bacillus pasteurii* on the nucleation and growth of calcium carbonate. *Geomicrobiol. J.* **23**, 213–226 (2006).
12. Warren, L. A., Mauri, P. A., Parmar, N. & Ferris, F. G. Microbially mediated calcium carbonate precipitation: Implications for interpreting calcite precipitation and for solid-phase capture of inorganic contaminants. *Geomicrobiol. J.* **18**, 93–115 (2001).
13. Pavez, J., Silva, J. F. & Melo, F. *Electrochim. Acta* **50**, 3488–3494 (2005).
14. Azizi, Z. *et al. J. Cluster Sci.* **27**, 1613–1628 (2016).
15. Rodriguez-Blanco, J. D., Shaw, S. & Benning, L. G. The kinetics and mechanisms of amorphous calcium carbonate (ACC) crystallization to calcite, viavaterite. *Nanoscale* **3**(1), 265–271 (2011).
16. Zou, Z. *et al.* A hydrated crystalline calcium carbonate phase: Calcium carbonate hemihydrate. *Science* **363**, 396–400. https://doi.org/10.1126/science.aav0210 (2019).
17. Clarà Saracho, A. *et al.* Characterisation of $CaCO_3$ phases during strain-specific ureolytic precipitation. *Sci. Rep.* **10**, 10168. https://doi.org/10.1038/s41598-020-66831y (2020).
18. Belcher, A. M. *et al.* Control of crystal phase switching and orientation by soluble mollusc-shell proteins. *Nature* **381**(6577), 56–58 (1996).
19. Christy, A. G. A review of the structures of vaterite: The impossible, the possible, and the likely. *Cryst. Growth Des.* **17**(6), 3567–3578 (2017).
20. Noskov, R. E., Shishkin, I. I., Barhom, H. & Ginzburg, P. Non-mie optical resonances in anisotropic biomineral nanoparticles. *Nano-scale* **10**(45), 21031–21040 (2018).
21. Cai, A. *et al.* Cho, Direct synthesis of hollow vaterite nanospheres from amorphous calcium carbonate nanoparticles via phase transformation. *J. Phys. Chem. C* **112**, 11324–11330 (2008).
22. Sackey, J. *et al.* Analysis of the miscibility of Cd^{2+} ions in $CaCO_3$. *Surf. Interfaces* **17**, 100356 (2019).
23. Trushina, D. B., Bukreeva, T. V., Kovalchuk, M. V. & Antipina, M. N. $CaCO_3$ vaterite microparticles for biomedical and personal care applications. *Mater. Sci. Eng. C* **45**, 644–658 (2014).
24. Antipina, M. N. & Sukhorukov, G. B. Remote control over guidance and release properties of composite polyelectrolyte based capsules. *Adv. Drug Delivery Rev.* **63**(9), 716–729 (2011).
25. Delce, M., Möhwald, H. & Skirtach, A. G. Stimuli-responsive LbL capsules and nanoshells for drug delivery. *Adv. Drug Delivery Rev.* **63**(9), 730–747 (2011).
26. Parakhonskiy, B. V., Yashchenok, A. M., Konrad, M. & Skirtach, A. G. Colloidal micro-and nano-particles as templates for polyelec-trolyte multilayer capsules. *Adv. Colloid Interface Sci.* **207**, 253–264 (2014).
27. Beuvier, T. *et al.* Synthesis of hollow vaterite $CaCO_3$ microspheres in supercritical carbon dioxide medium. *J. Mater. Chem.* **21**(26), 9757 (2011).
28. Vance, K. *et al.* Direct carbonation of Ca(OH)2 using liquid and supercritical CO2: Implications for carbon-neutral cementation. *Ind. Eng. Chem. Res.* **54**, 8908–8918 (2015).
29. Sargheini, J. *et al.* One-step facile synthesis of $CaCO_3$ nanoparticles via mechano-chemical route. *Powder Technol.* **219**, 72–77 (2012).
30. Shih, S.-M., Ho, C.-S., Song, Y.-S. & Lin, J.-P. Kinetics of the reaction of $Ca(OH)_2$ with CO_2 at low temperature. *Ind. Eng. Chem. Res.* **38**(4), 1316 (1999).
31. Lopez-Periago, A. M., Pacciani, R., García-Gonzalez, C., Vega, L. F. & Domingo, C. A breakthrough technique for the preparation of high-yield precipitated calcium carbonate. *J. Supercrit. Fluids* **52**(3), 298 (2010).
32. Montes-Hernandez, G., Renard, F., Geoffroy, N., Charlet, L. & Pironon, J. Calcite precipitation from CO_2–H_2O–Ca $(OH)_2$ slurry under high pressure of CO_2. *J. Cryst. Growth* **308**(1), 228 (2007).
33. Sadowski, Z., Polowczyk, I., Frąckowiak, A., Kozlecki, T. & Chibowski, S. Bio inspired synthesis of calcium carbonate colloid particles. *Physicochem. Probl. Miner. Process.* **44**, 205–214 (2010).
34. Enyedi, N. T. *et al.* Cave bacteria-induced amorphous calcium carbonate formation. *Sci. Rep.* **10**, 8696 (2020).
35. Veis, A. A window on biomineralization. *Science* **307**(5714), 1419 (2005).
36. Garg, R. *et al.* Green synthesis of calcium carbonate nanoparticles using waste fruit peel. *Mater. Today Proc.* (2022).
37. Yugandhar, P. & Savithramma, N. Green synthesis of calcium carbonate nanoparticles and their effects on seed germination and seedling growth of *Vigna mungo* (L.). *Int. J. Adv. Res.* **1**(8), 89–103 (2013).
38. Yao, L. *et al.* Green synthesis of calcium carbonate with unusual morphologies in the presence of fruit extracts. *J. Chil. Chem. Soc.* **58**, 4 (2013).
39. Chen, L. *et al.* Green synthesis of calcium carbonate uniform microspheres using vegetables. *Chin. J Chem.* **30**(2), 445–448 (2012).
40. Chuzeville, L. *et al.* Eco-friendly processes for the synthesis of amorphous calcium carbonate nanoparticles in ethanol and their stabilisation in aqueous media. *Green Chem.* **24**, 1270 (2020).

41. Uzunoğlu, D. & Özer, A. Biosynthesis and characterization of $CaCO_3$ nanoparticles from the leach solution and the aqueous extract of Myrtus communis plant. *Int. Adv. Res. Eng. J.* **02**(03), 245–253 (2018).
42. Khatami, M. *et al.* Calcium carbonate nanowires: Greener biosynthesis and their leishmanicidal activity. *RSC Adv.* **10**, 38063 (2020).
43. Bahrom, H. *et al.* Controllable synthesis of calcium carbonate with different geometry: comprehensive analysis of particle formation, cellular uptake, and biocompatibility. *ACS Sustain. Chem. Eng.* **7**, 19142–19156 (2019).
44. Nurul Islamet, K. *et al.* Facile synthesis of calcium carbonate nanoparticles from cockle shells. *J. Nanomater.* **2012**, 534010. https://doi.org/10.1155/2012/534010 (2012).
45. Yugandhar, P. & Savithramma, N. Green synthesis of calcium carbonate nanoparticles and their effects on seed germination and seedling growth of *Vigna mungo* (L.). *Hepper. Int. J. Adv. Res.* **1**(8), 89–103 (2013).
46. Chen, L. *et al.* Bacteria-mediated synthesis of metal carbonate minerals with unusual morphologies and structures. *Crystal Growth Des.* **9**(2), 743–754 (2009).
47. Thovhogi, N. *et al.* Journal, Physical properties of CdO nanoparticles synthesized by green chemistry via Hibiscus Sabdariffa flower extract. *J. Alloys Compounds* **655**, 314–320 (2016).
48. Thema, F. T. *et al.* Single phase Bunsenite NiO nanoparticles green synthesis by *Agathosma betulina* natural extract. *J. Alloys Compounds* **657**, 655–661 (2016).
49. Khalil, A. T. *et al.* Biosynthesis of iron oxide (Fe2O3) nanoparticles via aqueous extracts of *Sageretia thea* (Osbeck.) and their pharmacognostic properties. *Green Chem. Lett. Rev.* **10**(4), 186–201 (2017).
50. Mohamed, H. E. A. *et al.* Biosynthesis of silver nanoparticles from *Hyphaene thebaica* fruits and their in vitro pharmacognostic potential. *Mater. Res. Express* **6**(10), 1050 (2019).
51. Mohamed, H. E. A. *et al.* Bio-redox potential of *Hyphaene thebaica* in bio-fabrication of ultrafine maghemite phase iron oxide nanoparticles (Fe2O3 NPs) for therapeutic applications. *Mater. Sci. Eng., C* **112**, 110890 (2020).
52. Mohamed, H. E. A. *et al.* Hytosynthesis of BiVO4 nanorods using *Hyphaene thebaica* for diverse biomedical applications. *AMB Express* **9**, 1–14 (2019).
53. Mohamed, H. E. A. *et al.* Structural, morphological and biological features of ZnO nanoparticles using *Hyphaene thebaica* (L) Mart. fruits. *J. Inorg. Organom. Polym. Mater.* **30**, 3241–3254 (2020).
54. Mohamed, H. E. A. *et al.* Optical properties of biosynthesized nanoscaled Eu2O3 for red luminescence applications. *J. Opt. Soc. Am. A* **37**(11), C73–C79 (2020).
55. Mohamed, H. E. A. *et al.* Green synthesis of CuO nanoparticles via *Hyphaene thebaica* extract and their optical properties. *Mater. Today Proc.* **36**, 591–594 (2021).
56. Mohamed, H. E. A. *et al.* Biosynthesis and characterization of CaZrO3 nanoparticles via *Hyphaene thebaica*: Effect of preparation method on morphology, electrical, and dielectric properties. *J. Mater. Sci. Mater. Electron.* **31**, 10018–10030 (2020).
57. Mohamed, H. E. A. *et al.* Physicochemical and nanomedicine applications of phyto-reduced erbium oxide (Er_2O_3) nanoparticles. *AMB Express* **13**(1), 24 (2023).
58. Mohamed, H. E. A. *et al.* Green synthesis of $CdWO_4$ nanorods with enhanced photocatalytic activity utilizing *Hyphaene thebaica* Fruit. *Chem. Select* **7**(39), e202201442 (2022).
59. Andrews, K. W. An X-ray examination of a sample of pure calcite and of solid-solution effects in some natural calcites. *Miner. Mag. J. Miner. Soc.* **29**, 85–99 (1950).
60. Markgraf, S. A. & Reeder, R. J. High-temperature structure refinements of calcite and magnesite. *Am. Miner.* **70**, 590–600 (1985).
61. Rodriguez-Navarro, C. *et al.* Thermal decomposition of calcite: Mechanisms of formation and textural evolution of CaO nanocrystals. *Am. Miner.* **94**, 578–593 (2009).
62. Kristova, P., Hopkinson, L. J. & Rutt, K. J. The effect of the particle size on the fundamental vibrations of the [CO32–] anion in calcite. *J. Phys. Chem. A* **119**(20), 1 (2015).
63. Gao, J. *et al.* structural modifications of single-crystal aragonite CaCO3 beginning at ~15 GPa: In situ vibrational spectroscopy and X-ray diffraction evidence. *Minerals* **10**, 924. https://doi.org/10.3390/min10100924 (2020).
64. Zhuravlev, Y. N. & Atuchin, V. V. First-principle studies of the vibrational properties of carbonates, under pressure. *Sensors* **21**(11), 3644 (2021).
65. Vagenas, N. V., Gatsouli, A. & Kontoyannis, C. G. Quantitative analysis of synthetic calcium carbonate polymorphs using FT-IR spectroscopy. *Talanta* **59**, 831–836 (2003).
66. de la Pierre, M. The Raman spectrum of $CaCO_3$ polymorphs calcite and Aragonite: A combined experimental and computational study. *J. Chem. Phys.* **140**, 164509 (2014).
67. Habermann, D., Neuser, R. D. & Richter, D. K. Low limit of Mn2+-activated cathodoluminescence of calcite: State of the art. *Sed. Geol.* **116**, 13–24 (1998).
68. Gaft, M., Nagli, L., Panczer, G., Waychunas, G. & Porat, N. The nature of unusual luminescence in natural calcite $CaCO_3$. *Am. Miner.* **93**, 158–167 (2008).
69. Calderón, T., Aguilar, M., Jaque, F. & Coy-Yll, R. Thermoluminescence from natural calcites. *J. Phys. C Solid State Phys.* **17**, 2027–2038 (1984) (Kettle aragonite instead precipitates at lower temperature out of boiling water, and involves the rapid precipitation of needle-shaped crystals that are likely characterized by a high density of structural defects18, hence the blue luminescence).
70. Toffolo, M. B., Regev, L., Dubernet, S., Lefrais, Y. & Boaretto, E. FTIR-based crystallinity assessment of aragonite-calcite mixtures in archaeological lime binders altered by diagenesis. *Minerals* **9**, 121 (2019).
71. Toffolo, M. B. *et al.* Luminescence reveals variations in local structural order of calcium carbonate polymorphs formed by different mechanisms. *Sci. Rep.* **9**, 16170. https://doi.org/10.1038/s41598-019-52587-7 (2019).
72. Besson, R. & Favergeon, L. Understanding the mechanisms of CaO carbonation: Role of point defects in CaCO3 by atomic-scale simulations. *J. Phys. Chem. C* **118**(39), 22583 (2014).
73. Graf, D. L. Crystallographic tables for the rhombohedral carbonates: American Mineralogist. *J. Earth Planet. Mater.* **46**, 1283–1316 (1961).
74. Sulimaia, N. H. *et al.* Facile synthesis of CaCO3 and investigation on structural and optical properties of high purity crystalline calcite. *Mater. Sci. Eng., B* **243**, 78–85 (2019).
75. Zepeng, Y. T. *et al.* CaCO3 as a new member of high solar-reflective filler on the cooling property in polymer composites. *J. Vinyl Addit. Technol.* **27**(2), 1. https://doi.org/10.1002/vnl.21801 (2019).
76. Pfaff, G. White pigments. *J. Phys. Sci. Rev.* **6**(12), 11–83. https://doi.org/10.1515/psr-2020-0202 (2020).
77. Baer, D. R. & Blanchard, D. L. *Appl. Surf. Sci.* **72**, 295 (1993).
78. Hossain, F. M., Murch, G. E., Belova, I. V. & Turner, B. D. Electronic, optical and bonding properties of $CaCO_3$ calcite. *Solid State Commun.* **149**, 1201–1203 (2009).
79. Jabeen, N. *et al.* Optimised synthesis of ZnO-nano-fertiliser through green chemistry: Boosted growth dynamics of economically important *L. esculentum*. *IET Nanobiotechnol.* **12**(4), 405–411 (2018).
80. Savithramma, N. Influence of calcium supply on biomass production of endemic and endangered tree species of Tirumala hills of South Eastern Ghats. *J. Indian Bot. Soc* **81**, 323–326 (2002).
81. Savithramma, N. Influence of calcium supply on photosynthetic rate in relation to calmodulin in endemic and endangered tree saplings of Seshachalam hills of South Eastern Ghats of India. *J. Plant Biol* **31**, 159–164 (2004).

82. Savithramma, N., Fareeda, G., Madhavi, V. & Murthy, S. S. D. Effect of calcium on photochemical activities of green leafy vegetables. *J. Plant Biol.* **34**(2), 95–98 (2007).
83. Savithramma, N. & Swamy, P. M. Uptake and distribution of calcium in groundnut (*Arachis hypogeae* L.) cultivars during pod development. *Indian J. Plant Physiol.* **38**, 28–33 (1995).
84. Savithramma, N., Yugandhar, P., Prasad, K. S., Ankanna, S. & Chetty, K. M. Ethnomedicinal studies on plants used by Yanadi tribe of Chandragiri reserve forest area, Chittoor District, Andhra Pradesh India. *J. Intercult. Ethnopharmacol.* **5**(1), 49 (2016).
85. Gandhi, N., Shruthi, Y., Sirisha, G., & Anusha, C.R. Facile and eco-friendly method for synthesis of calcium oxide (CaO) nanoparticles and its potential application in agriculture. Haya Saudi J. Life Sci. ISSN 2415-623X |ISSN 2415-6221. https://doi.org/10.36348/sjls.2021.v06i05.003 (2021).
86. Taylor, H. F. W. *Cement Chemistry* (Thomas Telford, 1997).
87. Daval, D. *et al.* Carbonation of Ca-bearing silicates, the case of wollastonite: Experimental investigations and kinetic modeling. *Chem. Geol.* **265**(1–2), 63 (2009).
88. De Muynck, W., De Belie, N. & Verstraete, W. Microbial carbonate precipitation in construction materials: A review. *Ecol. Eng.* **36**(2), 118 (2010).
89. Jonkers, H. M. Self healing concrete: A biological approach. In *Self healing materials* (ed. van der Zwaag, P. S.) 195–204 (Springer Series in Materials Science, 2007).
90. Al-Thawadi, S. *High strength in-situ biocementation of soil by calcite precipitating locally isolated ureolytic bacteria* (Murdoch University, 2008).
91. Al-Thawadi, S. M. Ureolytic bacteria and calcium carbonate formation as a mechanism of strength enhancement of sand. *J. Adv. Sci. Eng. Res.* **1**(1), 98 (2011).
92. Ariyanti, D. & Handayani, N. A. Feasibility of using microalgae for biocement production through biocementation. *J. Bioprocess. Biotech.* **02**(01), 1–4 (2012).
93. Hendriks, C. A., Worrell, E., De Jager, D., Blok, K. & Riemer, P. Emission reduction of greenhouse gases from the cement industry. *Int. Energy Agency IEA* **939**, 1 (2002).
94. Worrell, E., Price, L., Martin, N., Hendriks, C. & Meida, L. O. Carbon dioxide emissions from the global cement industry. *Annu. Rev. Energy Environ.* **26**(1), 303 (2001).
95. Lee, T. & Lee, J. Evaluation of chloride resistance of early-strength concrete using blended binder and polycarboxylate-based chemical admixture. *Appl. Sci.* **10**, 2972. https://doi.org/10.3390/app10082972 (2020).
96. Kana, N., Khamlich, S., Kana Kana, J. B. & Maaza, M. Peculiar surface size-effects in NaCl nano-crystals. *Surf. Rev. Lett.* **20**(1), 1350001 (2013).
97. Maaza, M., Henini, M., & Ezema, F., *et al.* Peculiar size effects in nanoscaled systems. *Nano-Horizons*. https://doi.org/10.25159/NanoHorizons.9d53e2220e31.
98. Yuki Kezuka, Y., Kawai, K., Eguchi, K. & Tajika, M. Fabrication of single-crystalline calcite needle-like particles using the aragonite-calcite phase transition. *Minerals* **7**(8), 133 (2017).
99. Wang, P. F. *et al.* Fucoidan-mediated anisotropic calcium carbonate nanorods of pH-responsive drug release for antitumor therapy. *Front. Bioeng. Biotechnol. Sec. Biomater.* **10**, 1 (2022).
100. Nakayama, M., Kajiyama, S., Nishimura, T. & Kato, T. Liquid-crystalline calcium carbonate: Biomimetic synthesis and alignment of nanorod calcite. *Chem. Sci.* **6**, 6230 (2015).
101. Babou-Kammoe, R., Hamoudi, S., Larachi, F. & Belkacem, Kh. Synthesis of $CaCO_3$ nanoparticles by controlled precipitation of saturated carbonate and calcium nitrate aqueous solutions. *Can. J. Chem. Eng.* **90**, 1 (2012).
102. Watanabe, H. *et al.* Effect of initial pH on formation of hollow calcium carbonate particles by continuous CO_2 gas bubbling into $CaCl_2$ aqueous solution. *Adv. Powder Technol.* **20**, 89–93 (2009).

Acknowledgements

We are grateful to the various supporting institutions including, the University of South Africa, iThemba LABS (ITLABS), the National Research Foundation of South Africa (NRF), the African Laser Centre (ALC), the international Organization of Women in Science (OWSD), the Abdus Salam International Centre for Theoretical Physics (The Abdus Salam-ICTP), the Royal Society-London and naturally the United Nations Education, Sciences and Culture Organization (UNESCO) as well as the French Foreign Ministry and the ADESFA program. Likewise, the Centre for High Performance Computation (CHPC) is acknowledged.

Author contributions

H.M.: Synthesis & various Experiments, KH: Synthesis & various characterizations, N.B.: Optical characterization studies,K.C.: Morphological & elemental investigations, S.A.: Crystallographic investigations, A.A.Q.: Preliminary Toxicity studies, R. M.: Computations & Modelling, Th.M.: Nanofertilizers studies, A.K. : Chemistry guidance, A.G. : Crystallographic studies guidance & analysis, M. H. : Manuscript reading & corrections, M.C.: Critical advisory, I.A.: Preliminary Nanofertilizers studies, M. M.: Concept, Data Analysis & Manuscript Writing.

Competing interests

The authors declare no competing interests.

Additional information

Supplementary Information The online version contains supplementary material available at https://doi.org/10.1038/s41598-023-42905-5.

Correspondence and requests for materials should be addressed to M.M.

Reprints and permissions information is available at www.nature.com/reprints.

Publisher's note Springer Nature remains neutral with regard to jurisdictional claims in published maps and institutional affiliations.